


## Article

# Highlights from GERDA: Probing the Majorana Neutrino Mass at 100 meV<sup>†</sup>

Carla Maria Cattadori<sup>‡</sup>  on behalf of the GERDA Collaboration

Piazza della Scienza, 3-20154 Milano, Italy; carla.cattadori@lngs.infn.it

<sup>†</sup> This paper is based on the talk at the 7th International Conference on New Frontiers in Physics (ICNFP 2018), Crete, Greece, 4–12 July 2018.

<sup>‡</sup> INFN Milano Bicocca.

Received: 19 December 2018; Accepted: 31 January 2019; Published: 7 February 2019



**Abstract:** Since 2010, the GERDA experiment at Laboratori Nazionali del Gran Sasso (LNGS) operates searching for neutrinoless double beta decay ( $0\nu\beta\beta$ ) of  $^{76}\text{Ge}$  to the ground and excited states of  $^{76}\text{Se}$ .  $0\nu\beta\beta$  is an ultra-rare process whose detection would directly establish the Majorana nature of the neutrino and provide a direct measurement of its mass. Since the apparatus upgrade in 2013–2015, the collaboration released the third update of the achieved results at the Neutrino 2018 Conference. The hardware upgrade and the fine tuning of the powerful analysis tools to reconstruct the event energy and to discriminate the background allowed the achievement of the energy resolution of 3 keV and 3.6 keV for Broad Energy Germanium (BEGE) and Coaxial Germanium (COAX) detectors, respectively, and an unprecedented low background index of  $0.6 \cdot 10^{-3}$  cts/(keV·kg·yr) in a 230 keV netto range centered at  $Q_{\beta\beta}$  in the exposure of 58.93 kg·yr. No evidence of the  $0\nu\beta\beta$  decay is found at the  $Q_{\beta\beta} = 2039.1$  keV, and the limit of  $0.9 \cdot 10^{26}$  yr on the half-life ( $T_{1/2}^{0\nu}$ ) at 90% C.L. is set. This corresponds to the limit range for the effective Majorana neutrino mass  $m_{ee}$  of 110–260 meV. The GERDA sensitivity in terms of background index, energy resolution and exposure is the best achieved so far in  $^{76}\text{Ge}$  double beta decay experiments, the energy resolution and background in the Region Of Interest (ROI) allow GERDA to operate in a background-free regime and to set a world record.

**Keywords:** neutrino; majorana; GERDA; Double Beta Decay; germanium

## 1. Introduction

The last two decades of particle experimental physics have showed that neutrinos, while propagating, oscillate one into the other: this is because they have a finite mass, and the three neutrino flavor eigenstates do not coincide with the three mass eigenstates. The parameters driving the oscillations, i.e., the three neutrino mass differences ( $\Delta m^2$ ) and the three oscillation mixing angles, have been measured with improving accuracy [1] although not at the 1% level as in the quark sector: the Majorana CP-violating phases instead are still unknown, as well as the octant of  $\theta_{23}$ . Unfortunately, these experiments cannot establish if the neutrino is a Dirac or Majorana particle and measure its absolute mass, and so far have not provided information on the eigenstates mass order (hierarchy). Some (weak) preference for the normal hierarchy order, i.e., largest splitting between the second and the third mass states, has been very recently provided by SuperKamioKande [2], under some assumptions.  $0\nu\beta\beta$  decay experiments instead probe lepton number conservation and the neutrino Dirac or Majorana nature: its (non) observation allows (limited) measurement of the absolute neutrino mass and indicates the neutrino mass hierarchy (normal, inverted, or quasi-degenerate). Massive Majorana neutrinos may acquire mass through the See-Saw mechanism [3], hence playing a main role in the Matter-Antimatter asymmetry of the Universe.

In many extensions of the Standard Model (SM), Double Beta Decay is supposed to occur in two modes: the two neutrino ( $2\nu\beta\beta$ ), allowed in SM, first detected on  $^{82}\text{Se}$  [4], today observed in 13 nuclei [5,6], and the zero neutrino ( $0\nu\beta\beta$ ), not allowed in the SM, so far unobserved despite being the object of searches with increasing experimental sensitivity for about 60 years: its quenching may be related to CP-violating phase cancellations, or to the quenching of the coupling constant  $g_A$ , of the Nuclear Matrix Elements (NME) associated with the nuclear transition, or if neutrinos are Dirac fermions.

GERDA was designed to first reach (Phase I), a background index (BI) of  $10^{-2}$  cts/(keV·kg·yr), aiming to test the controversial claim of  $0\nu\beta\beta$  detection by the HDM experiment [7], while proving the feasibility of the GERDA innovative operation of the HP-Ge detectors, originally proposed by [8]. Since its proposal in 2004, it was foreseen to proceed to a second phase Phase II improving the BI down to  $10^{-3}$  cts/(keV·kg·yr). Figure 1 shows the GERDA design sensitivity on the  $0\nu\beta\beta$  half-life ( $T_{1/2}^{0\nu}$ ), as a function of the exposure and for different BI. From the exponential decay law and Poisson statistics it directly follows that in presence of background, i.e., when in the experimental lifetime a number  $N > 1$  of events (cts) is expected in the Region Of Interest (ROI) from the integral of background sources, the  $T_{1/2}^{0\nu}$  sensitivity scales with the square root of the exposure, i.e.,  $T_{1/2}^{0\nu} \sim \sqrt{\frac{\mathcal{E}}{BI \cdot \Delta E}}$ , while when operating in background-free condition ( $N < 1$  cts in the ROI in the experimental lifetime)  $T_{1/2}^{0\nu}$  scales linearly with the exposure ( $\sim \sqrt{\mathcal{E}}$ ).

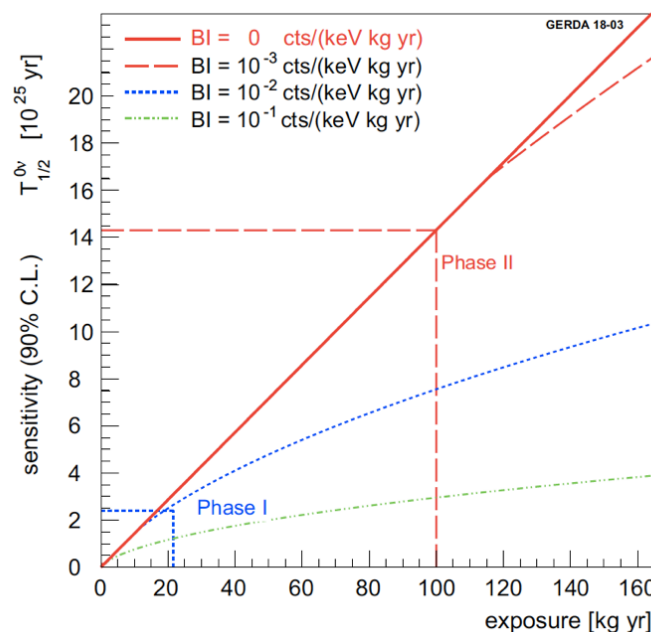


**Figure 1.** The GERDA sensitivity on the  $0\nu\beta\beta$  half-life ( $T_{1/2}^{0\nu}$ ) of  $^{76}\text{Ge}$  as a function of the exposure and for different BI.

## 2. The Setup

The GERDA experimental lifetime is divided in two phases, as the setup underwent significant changes in between:

- Phase I was operated from 9 November 2011 to August 2013. Eight semi-coaxial germanium (COAX) detectors enriched up to  $\sim 87\%$  in  $^{76}\text{Ge}$  ( $^{76}\text{Ge}^{\text{enr}}$ ) from the former Heidelberg-Moscow (HDM) [9] and Igex (IGEX) [10] experiments, and later 5 freshly produced  $^{76}\text{Ge}^{\text{enr}}$  point-contact germanium detectors (BEGE), for a total mass of  $\sim 18$  kg of  $^{76}\text{Ge}^{\text{enr}}$ , were operated bare in a  $63 \text{ m}^3$  liquid argon (LAr) bath. The LAr cryostat is in turn placed at the center of a  $650 \text{ m}^3$  water tank where a Cerenkov muon veto detector is installed. The experimental setup is fully described in [11].

- Phase II started on 20 December 2015 after 1.5 years of upgrade work: the  $^{\text{enr}}\text{Ge}$  mass increased up to 35.6 kg, 20 kg in form of 20 BEGE detectors [12], 19 of which were properly functioning, the rest being the Phase I  $^{\text{enr}}\text{Ge}$ -COAX detectors (15.6 kg) plus 3  $^{\text{nat}}\text{Ge}$ -COAX (7.6 kg). It was shown [13] that the BEGE detectors have improved pulse shape rejection features with respect to COAX: this is thanks to the highly non-uniform electric field, yielding to a large spread and gradient of the holes drift velocities in the detector volume, hence to longer and more stretched pulses, allowing better discrimination of multi-site (MSE) energy releases. The pulse shape discrimination of Compton scattered  $\gamma$ s is hence improved. In addition, to reject those  $\gamma$ s releasing energy in the Ge detectors after scattering in LAr, a volume of  $\sim 50$  cm diameter and  $\sim 220$  cm height was delimited by an Oxygen Free High Conductivity (OFHC) Cu foil lined with a reflector foil and equipped with 16 Photomultipliers (9 top, 7 bottom): the central 100 cm of the cylinder are equipped with 800 m Scintillating Fibers, replacing the Cu foil, read out by Silicon Photo Multipliers (SiPM).

To further confine the LAr in intimate contact with the Ge detectors, hence minimize the rate of the extremely dangerous  $\sim 3.5$  MeV  $\beta$  particles from  $^{42}\text{K}$  decaying at the detector surface<sup>1</sup>, a transparent mini-shroud made from the Borexino ultra-low radioactivity nylon [14], surrounds each detector string.  $^{42}\text{K}$  is a cosmogenic isotope contained in LAr at  $\mathcal{O}(100)$   $\mu\text{Bq}$  level. The mini-shrouds, the fibers, the reflector foils, the PMTs are coated with TPB<sup>2</sup> a VUV wavelength shifter, shifting the 128 nm LAr scintillation light to match the PMTs and SiPM spectral sensitivity in the optical range. The Phase II array, the nylon mini-shrouds and the fiber curtain shroud are shown in Figure 2 and described in [15].



**Figure 2.** The Phase II Ge array with the individual Ge detector strings inserted in TPB coated nylon mini-shrouds (left) and the Fiber Shroud surrounding the detector strings once lifted up in the lock (right).

Both the energy scale and the energy resolution (FWHM) of the Ge detectors are bi-weekly calibrated lowering three  $^{228}\text{Th}$  sources that are permanently installed in the apparatus and can be remotely lowered into the cryostat down to the array level.

<sup>1</sup>  $^{42}\text{K}$  ( $T_{1/2} = 12.6$  h;  $(\beta^- - \gamma)$ ) is the decay product of  $^{42}\text{Ar}$  ( $T_{1/2} = 32.9$  y;  $\beta^-$ )

<sup>2</sup> TPB: Tetraphenyl butadiene

The LAr veto is also calibrated, with  $^{226}\text{Ra}$  and  $^{228}\text{Th}$  sources of reduced intensity, about once/twice per year.

### 3. Data Taking

Phase I data taking was stopped when reaching the exposure of 21.6 kg·yr (detector mass), corresponding to 234 mol·y of  $^{\text{enr}}\text{Ge}$  [16]; as the achieved BI of  $10^{-2}$  cts/(keV·kg·yr) did not match the zero-background condition, the sensitivity would be soon dominated by background fluctuations and slowly increase with the square root of the exposure, as illustrated in Figure 1.

Phase II started in December 2015, aiming to improve the BI by a factor 10 regarding Phase I, and is ongoing. At the time of writing, an  $\mathcal{E} = 58.93$  kg·yr of  $^{\text{enr}}\text{Ge}$  corresponding to 593 mol·y of  $^{\text{enr}}\text{Ge}$  has been released, hence more than doubling the previously released exposure of 23.2 kg·yr [17,18]. The Phase II BI satisfies the design condition ( $\leq 10^{-3}$  cts/(keV·kg·yr)), as discussed in the following and reported in Table 1.

The data acquisition duty cycle is 92.9%, the fraction of valid data is 80.4%. The trigger threshold is  $\sim 200$  keV (recently lowered to  $\sim 30$  keV), the trigger condition being the OR of the Ge detectors. The LAr veto detector do not trigger the data acquisition, but it is read out at each Ge trigger.

**Table 1.** Parameters for the six data sets: “N” is the number of events in the 230 keV window centered at  $Q_{\beta\beta}$  and BI the respective background index, calculated as  $N/(\mathcal{E} \cdot 230 \text{ keV})$ .

Data Set	$\mathcal{E}$ [kg · yr]	FWHM [keV]	$\langle\epsilon\rangle$	BI $10^{-3}$ cts/(keV · kg · yr)	N
Phase I-Golden	17.9	4.3(1)	0.57(3)	$11 \pm 2$	46
Phase I-Silver	1.3	4.3(1)	0.57(3)	$30 \pm 10$	10
Phase I-BEGe	2.4	2.7(2)	0.66(2)	$5^{+4}_{-3}$	3
Phase I-Extra	1.9	4.2(2)	0.58(4)	$5^{+4}_{-3}$	2
Phase II-COAX 1	5.0	3.6(1)	0.52(4)	$3.5^{+2.1}_{-1.5}$	4
Phase II-COAX 2	23.1	3.6(1)	0.48(4)	$0.6^{+0.4}_{-0.3}$	3
Phase II-BEGe	30.8	3.0(1)	0.60(2)	$0.6^{+0.4}_{-0.3}$	5

### 4. Data Treatment

Data are divided in seven sets (see Table 2) corresponding to major hardware changes or to specific time periods. Four data sets in Phase I: (i) GOLDEN-COAX: all the coaxial data but two runs after the insertion of BEGe pilot string in July 2012; (ii) SILVER-COAX: the coaxial data from the two runs just after the BEGe string deployment; (iii) BEGe: all the BEGe data, (iv) Extra: the COAX data collected after the Phase I unblinding, and before the setup upgrade to Phase II. Three data sets in Phase II: (v) COAX-1: from December 2015 to the first Phase II data release in 2016 [18]; (vi) COAX-2: from 2016 to April 2018 [17]; (vii) BEGe: all the BEGe data.

**Table 2.** The efficiency/fraction factors multiplying the mass term in the  $T_{1/2}^{0\nu}$  computation.

Data Set	Enrich.	Active Vol	Peak	QC	LAr-Veto	PSD	Total
Phase I-Golden	86.7	86.7	91.4	> 99	-	83(3)	57(3)
Phase I-Silver	86.7	86.6	91.4	> 99	-	83(3)	57(3)
Phase I-BEGe	87.8	91.0	90.0	> 99	-	92.1(1.9)	66(2)
Phase I-Extra	86.7	87.2	91.7	> 99	-	83(3)	58(4)
Phase II-COAX 1	86.7	86.5	91.4	99.92	97.8(1)	77(5)	52(4)
Phase II-COAX 2	86.6	86.4	91.4	99.92	97.7(1)	71.2(4.3)	48(4)
Phase II-BEGe	88.00	88.7	89.7	99.92	97.7(1)	87.6(2.5)	60(2)

The first step of the physics data analysis is the energy reconstruction: this is performed by first de-noising the recorded 160  $\mu\text{s}$  waveform, sampled at 40 ns, with a zero-area cusp-shaped

filter [19], whose relevant parameters are determined by optimizing the energy resolution of the most prominent  $^{228}\text{Th}$   $\gamma$  lines in the calibration spectra. It can be shown that the cusp (in the time domain) filter corresponds to an optimum filter in the frequency domain. The relevant cusp parameters are hence determined maximizing the S/N ratio. The energy-to-amplitude calibration parameters defined in the calibration data are then applied to the corresponding physics data. Figure 3 shows the *exposure-weighted* energy resolution<sup>3</sup> expressed in term of FWHM, as a function of the energy for both the BEGE and COAX detectors, and the matching of the energy scale and energy resolution between the calibration and the physics data. The energy resolution at  $Q_{\beta\beta}$  for both the Phase II-COAX and the single Phase II-BEGE data sets are 3.6 keV and 3.0 keV, respectively. The systematics related to the non-linearity of the energy scale are 0.2 keV.

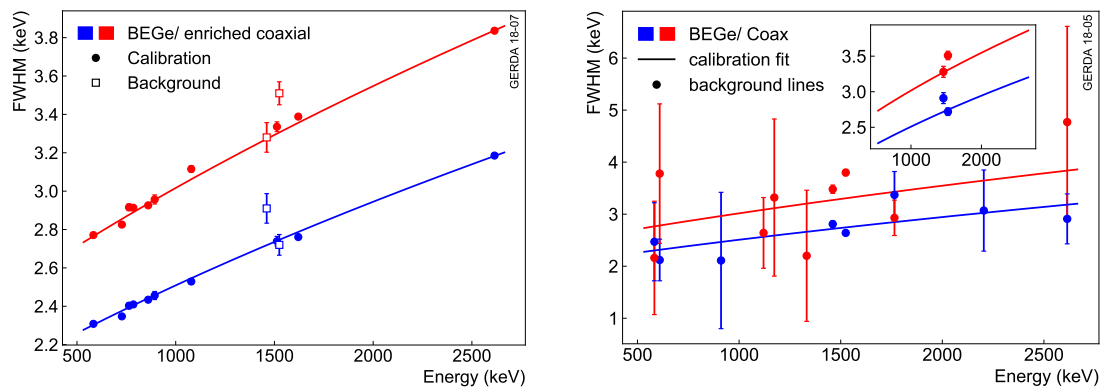


**Figure 3.** The energy resolution in Phase II as a function of the energy for both the BEGE and COAX detectors. (Left): The *exposure-weighted* FWHM of the  $\gamma$  lines adopted in the calibration vs. energy, and their fit function. The FWHM of the  $^{42}\text{K}$  and  $^{40}\text{K}$  lines in the physics data are superimposed; (Right): the FWHM of the gamma lines in the physics data, and, superimposed, the *exposure-weighted* FWHM function derived from the calibrations: the inset presents the *exposure-weighted* FWHM of the two most prominent  $^{42}\text{K}$  and  $^{40}\text{K}$  lines.

Once the energy is assigned and the energy spectra produced, the events with  $E > 500$  keV are processed as follows [20,21]; first, quality cuts are applied (acceptance is 99.92%) to remove fake triggers and triggers from electrostatic micro-discharges, then single multiplicity (only one detector above the DAQ trigger) (acceptance  $94.5 \pm 0.6\%$ ) and anti-coincidence within 1  $\mu\text{s}$  with the muon veto (acceptance  $93.7 \pm 0.6\%$ ) is required. When considering the 100 keV energy region around  $Q_{\beta\beta}$  the quality cut acceptance is unchanged within the errors while the anti-coincidence acceptances decreases to  $(66 \pm 7)\%$  and  $(60 \pm 7)\%$  respectively, due to the absence of the  $2\nu\beta\beta$  signal (intrinsically single hit), and the decrease of the full containment efficiency at the increase of the  $\gamma$ -energy.

Next, the anti-coincidence within 7  $\mu\text{s}$  with the LAr veto is required.

The last event-selection step is based on pulse shapes (PSD):  $0\nu\beta\beta$  is intrinsically a single-site event (SSE). To reject background by MSE, while preserving SSEs, different selection criteria and algorithms have been developed for COAX and BEGE. For the COAX the PSD cut is applied on the distribution of the pulse shape estimator, provided by an Artificial Neural Network (ANN) [21] & a cut on the pulse rise-time: pulses with rise-time<sup>4</sup> lower than 180 ns are rejected as associated with  $\alpha$  particles decaying at the  $p^+$  electrode. For the BEGE the PSD estimator is the ratio of the amplitudes of current pulse vs. charge pulse (A/E) [21].

<sup>3</sup> both the energy calibration and energy resolution have some  $\pm$  variations from one calibration to the other, usually  $\sim 0.1$ – $0.3$  keV, but in some cases, larger. Hence the physics data are calibrated following the scale variations and an *exposure-weighted* FWHM is determined for each data set

<sup>4</sup> time for the pulse from 10% to 90% of its amplitude



For both estimators, the events populating the 1592 keV  $\gamma$ -line (double escape peak of the 2614 keV,  $^{208}\text{Tl}$ ) and the full energy peaks (FEP) of the 1620 keV  $^{212}\text{Bi}$   $\gamma$ -line are proxies of  $0\nu\beta\beta$  (SSE) and background (MSE) respectively. The acceptances are then verified on other SSE classes of events, as  $2\nu\beta\beta$  and Compton edges.

For each data set, Table 2 reports the average of the enrichment fraction, the active volume and the associated containment  $0\nu\beta\beta$  fraction, as well as the individual estimated efficiencies (acceptances) on genuine SSE of the two cuts, LAr-veto and PSD.

For the  $0\nu\beta\beta$  analysis the 260 keV region centered at  $Q_{\beta\beta}$  excluding the blinded 50 keV energy window centered at  $Q_{\beta\beta}$  and the two regions  $(2104 \pm 5)$  keV and  $(2119 \pm 5)$  keV, corresponding to known  $\gamma$  lines of  $^{208}\text{Tl}$  and  $^{214}\text{Bi}$ , is adopted for the first determination of the BI.

After the cuts, the analysis criteria and the related efficiencies are determined, the 50 keV blinded region is unveiled, and the cuts are applied. The BI is re-evaluated on the 240 keV region excluding 10 keV at  $Q_{\beta\beta}$ , hence on a 230 keV netto range. To maximize the exposure while taking advantage of the different energy resolution, background indexes, and pulse shape discrimination (PSD) features of the individual detectors and time periods, the BIs determined in the 230 keV range of each data sets are free parameters in the unbinned maximum likelihood fit of the  $0\nu\beta\beta$  ROI, while the half-life of a Gaussian signal at  $Q_{\beta\beta}$ , is free and common to all the data sets: the  $T_{1/2}^{0\nu}$  is related to  $N_{\beta\beta}$ , through the  $T_{1/2}^{0\nu} = \ln 2 \cdot \frac{\epsilon \cdot N_{\text{Nuclei}} \cdot T_{\text{meas}}}{N_{\beta\beta}}$ .  $\epsilon$  is total measurement efficiency reported in Table 2.

Finally, the corresponding neutrino mass (limit) is computed, through the  $(T_{1/2}^{0\nu})^{-1} \sim F_{0\nu}(Q, Z) \cdot |M_{0\nu}|^2 \cdot \frac{\leq m_{ee}^2}{m_e^2}$ , where  $\langle m_{ee} \rangle$  is the effective Majorana Neutrino Mass,  $m_e$  is the electron mass,  $F_{0\nu}(Q, Z)$  is the transition phase space [22],  $M_{0\nu}$  is the Nuclear Matrix Element of the  $^{76}\text{Ge} \rightarrow ^{76}\text{Se}$  transition: NME calculations provide values ranging within a factor of 2–4 depending on adopted nuclear models [23]: a range of values for  $M_{0\nu}$  leads to a range for the neutrino mass limit.

## 5. Discussion and Results

The PSD cuts are tailored to reject MSE (like Compton scattering inside the detector),  $\alpha$ s and  $\beta$  decays at the detector surface; for BEGE this is achieved by low and high cut on A/E, the PSD parameter: in fact, the multi-site events show lower A/E than SSEs, while  $\alpha$ s decaying at the  $p^+$  electrode have high A/E. For COAX: the ANN cut removes the Compton events and to some extent the  $\alpha$ s, the rise-time cut removes more effectively the  $\alpha$ s.

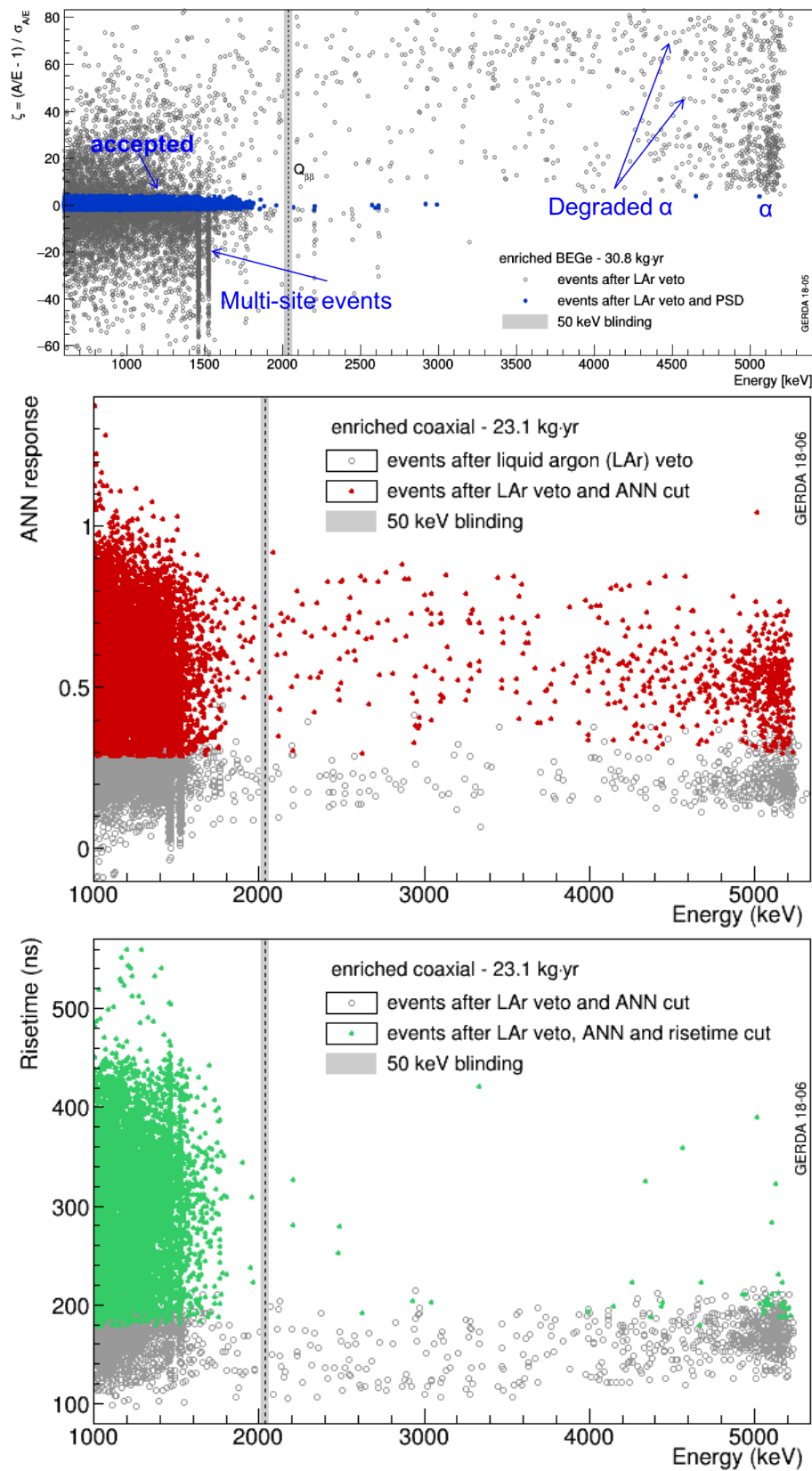
In Figure 4 plots, for each data set, the open gray circles represent the population of events prior the active cuts, plotted in the plane PSD estimator vs energy. The colored filled points are the events surviving the PSD cuts.

Prior to the cuts, BEGE detectors are shown to be 10 times cleaner in  $^{210}\text{Po}$  than COAX, and this is consistent with the reduced  $p^+$  electrode contact area.

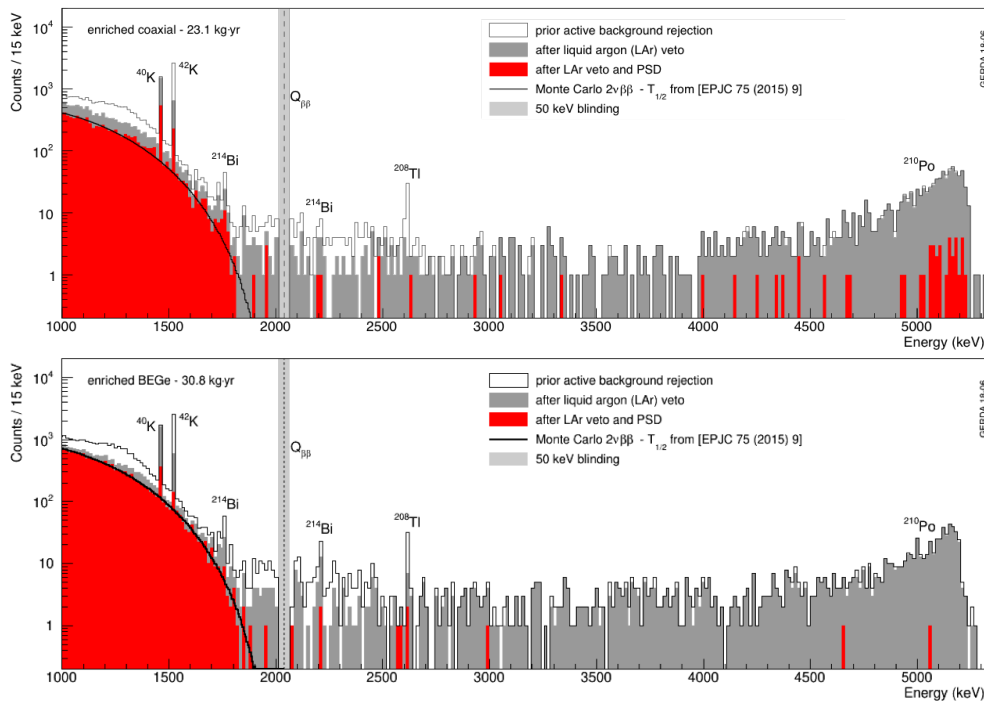
Figure 5 shows the energy spectra collected in Phase II before and after applying the active background rejection cuts, for both the  $^{\text{enr}}\text{Ge}$  BEGE and the  $^{\text{enr}}\text{Ge-coax}$ . Prior the cuts the spectral features are: (i)  $2\nu\beta\beta$  at  $E < 2.0$  MeV; (ii)  $^{40}\text{K}$ ,  $^{42}\text{K}$  prominent  $\gamma$  lines at 1.460 MeV and 1.525 MeV respectively,  $^{214}\text{Bi}$   $\gamma$  lines at 1.764 MeV, 2.2 MeV,  $^{208}\text{Tl}$   $\gamma$  line at 2.6 MeV; (iii)  $^{210}\text{Po}$   $\alpha$ s at  $\sim 5.2$  MeV extending down to lower energies (named *degraded  $\alpha$* , i.e., losing part of their energy in the detector dead layers). The LAr veto cut affects mostly the  $\gamma$  lines from  $\beta$ - $\gamma$  emitters ( $\beta$  in LAr and  $\gamma$  in the Ge detectors), abating  $\sim 80\%$  the  $^{42}\text{K}$  and  $^{214}\text{Bi}$  and to a minor extent ( $\sim 50\%$ ) their Compton continuum.

Table 1 summarizes the relevant parameters for each data set: exposure, energy resolution, total efficiency to SSE, BI and number of background events in the 230 keV range after the cuts: the BI of most of the Phase II exposure well satisfy the design value.

Only one event in the Phase II-BEGE data set is found at  $+2.4 \sigma$  from  $Q_{\beta\beta}$ , shown in Figure 6. The expected number of background counts for the three Phase II data sets in  $\pm \text{FWHM}$  is 0.32.



**Figure 4.** PSD estimators plotted vs. energy for Phase II BEGe (top) and COAX (middle) data sets: for COAX the rise-time parameter vs. the energy is also shown (bottom). The empty circles are all the events prior the active cuts, while the filled coloured circles are the events surviving the cut on the PSD estimator.



**Figure 5.** The GERDA Phase II energy spectra: 23.1 kg-yr for the COAX̃(top) and 30.8 kg-yr for the BEG̃E(bottom), for a total exposure of 58.93 kg-yr.

The unbinned maximum likelihood best fit value is a null signal; the maximum signal fitting the ROI is shown in Figure 6. The corresponding 90% C.L. limit is  $T_{1/2}^{0\nu} > 0.9 \cdot 10^{26}$  yr, and, in the assumption that neutrino is a Majorana particle, the neutrino mass upper limit ranges 0.11–0.26 eV. It is relevant to point out that if  $0\nu\beta\beta$  of  $^{76}\text{Ge}$  would proceed with the claimed half-life of  $1.2 \cdot 10^{25}$  yr [7] ( $2.2 \cdot 10^{25}$  yr in [24]), in GERDA Phase II a peak of  $\sim 15$  cts ( $\sim 8$  cts) will show up at  $Q_{\beta\beta}$ , while, under this assumption, the Poisson probability of founding 1 cts is  $< 10^{-5}$  ( $3.0 \cdot 10^{-3}$ ). Hence the GERDA results exclude both [7,24].

Also, the GERDA limit value is in good agreement with its median sensitivity for limit-setting computed by Toy Monte Carlo method:  $T_{1/2}^{0\nu} > 1.1 \cdot 10^{26}$  yr, leading to  $m_{ee} < 0.10$ –0.23 eV, and the probability of having a stronger limit is 63%.

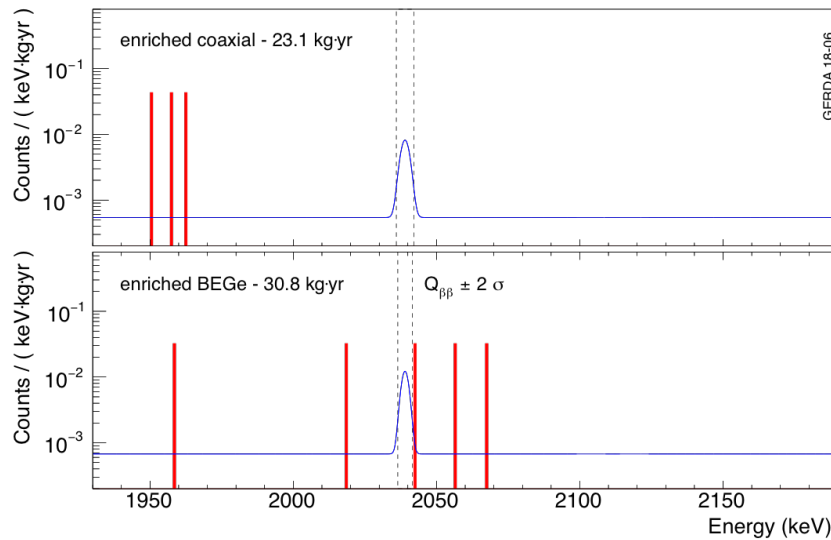


**Figure 6.** The GERDA Phase II energy spectra zoomed at the ROI for the COAX (top) and BEGE (bottom) data sets. Overlapped the maximal signal allowed from the maximum likelihood fit.



## 6. Conclusions

Presently, the more stringent results on  $0\nu\beta\beta$  are set on  $^{136}\text{Xe}$ ,  $^{76}\text{Ge}$ ,  $^{130}\text{Te}$ ,  $^{82}\text{Se}$  by the KAMLAND-ZEN, GERDA, CUORE, CUPID experiments, respectively. Table 3 summarizes these and a few other results: neutrinoless double beta decay half-lives  $\mathcal{O}(10^{26})$  yr, corresponding to (sub) 100 meV, i.e., the so-called degenerate region of the effective Majorana neutrino mass scale, is presently probed by a few projects, the most sensitive being the  $^{136}\text{Xe}$  and  $^{76}\text{Ge}$  ones. So far neither evidences nor indications of  $0\nu\beta\beta$  have been found, and the previous claim [7][24] has been disproved.

**Table 3.** Summary and comparison of the main parameters, performance, and results of the ongoing Double Beta Decay Experimental Searches.

	Isotope	Moles	$\mathcal{E}$ [kg · yr]	FWHM [keV]	BI·10 <sup>3</sup> cts/(keV · kg · yr)	Sensitivity $T_{1/2}^{0\nu}$ 10 <sup>25</sup> [yr]	Limit $T_{1/2}^{0\nu}$ 10 <sup>25</sup> [yr]	Limit Range [eV] $m_{ee}$
GERDA [? ]	$^{76}\text{Ge}$	410	59.3	3.3	0.6	11.0	9.0	0.11–0.26
MAJORANA [25]	$^{76}\text{Ge}$	340	26.0	2.5	5.0	4.8	1.9	0.24–0.52
CUORE [26]	$^{130}\text{Te}$	1580	83.6	7.7	15.0	0.7	1.5	0.11–0.52
CUPID [27]	$^{82}\text{Se}$	57	2.9	23.0	3.6	0.23	0.24	0.38–0.77
EXO-200 [28]	$^{136}\text{Xe}$	550	56	71	1.7	3.7	1.8	0.15–0.40
KAMLAND-ZEN [29]	$^{136}\text{Xe}$	2530	138	265	0.3	5.6	11.0	0.06–0.17

GERDA has validated its innovative technique of operating bare germanium detector in LAr, and proved that first-class physics results can be achieved, thanks to the best BI ( $0.6 \cdot 10^{-3}$  cts/(keV·kg·yr)) and energy resolution (FWHM: 3.0 keV for low capacity HP-Ge detectors) at  $Q_{\beta\beta}$ , and to the largest  $^{76}\text{Ge}$  exposure ever achieved in  $0\nu\beta\beta$  searches.

The next step in neutrinoless double beta decay searches will be the exploration of the inverted hierarchy region of the Majorana neutrino mass range (few tens of meV, corresponding to the  $10^{26}$ – $10^{27}$  yr range for the  $T_{1/2}^{0\nu}$ ): it is the goal of the LEGEND-200 project, proposed by the joint GERDA and MAJORANA collaborations, and of the KAMLAND-ZEN-800 projects. LEGEND-200 [30] aims to increase the detector mass to 150–200 kg in form of BEGe or Small Anode Germanium (SAGE) or Inverted Coaxial Germanium detectors, deploying the target in the GERDA infrastructure at LNGS, with a further reduced BI  $\leq 10^{-4}$  cts/(keV·kg·yr). The KAMLAND-ZEN-800 project will soon restart the operations with a doubled  $^{136}\text{Xe}$  isotope mass: at the time of writing (end of 2018), the internal balloon has already been deployed and filled with dummy liquid scintillator, without  $^{136}\text{Xe}$ .

Only multi-ton double beta decay experiments will have adequate sensitivity to probe the normal hierarchy neutrino mass ordering at a few meV scale, or the  $10^{28}$ – $10^{29}$  yr range for the  $T_{1/2}^{0\nu}$ .

**Funding:** This GERDA experiment is supported financially by the German Federal Ministry for Education and Research (BMBF), the German Research Foundation (DFG) via the Excellence Cluster Universe, the Italian Istituto Nazionale di Fisica Nucleare (INFN), the Max Planck Society (MPG), the Polish National Science Centre (NCN), the Russian Foundation for Basic Research (RFBR), and the Swiss National Science Foundation (SNF). The institutions acknowledge also internal financial support.

**Conflicts of Interest:** The authors declare no conflict of interest.

## References

1. Esteban, I.; Gonzalez-Garcia, M.C.; Maltoni, M.; Martinez-Soler, I.; Schwetz, T. Updated fit to three neutrino mixing: exploring the accelerator-reactor complementarity. *J. High Energ. Phys.* **2017**, 2017, 87.
2. Jiang, M. [SUPER-KAMIOKANDE Collaboration] Atmospheric Neutrino Oscillation Analysis With Improved Event Reconstruction in Super-Kamiokande IV. *arXiv* **2019**, arXiv:1901.03230.
3. Mohapatra, R.N.; Senjanović, G. Neutrino Mass and Spontaneous Parity Non-conservation. *Phys. Rev. Lett.* **1980**, 44, 912.
4. Elliott, S.R.; Hahn, A.A.; Moe, M.K. Direct evidence for two-neutrino double-beta decay in  $^{82}\text{Se}$ . *Phys. Rev. Lett.* **1987**, 59, 2020.
5. Barabash, A.S. Main features of detectors and isotopes to investigate double beta decay with increased sensitivity. *Int. J. Mod. Phys. A* **2018**, 33, 1843001.

6. Alduino, C. et al. [CUORE Collaboration] Low Energy Analysis Techniques for CUORE. *Eur. Phys. J. C* **2017**, *77*, 13.
7. Klapdor-Kleingrothaus, H.V.; Krivosheina, I.V.; Dietz, A.; Chkvorets, O. Search for neutrinoless double beta decay with enriched  $^{76}\text{Ge}$  in Gran Sasso 1990–2003. *Phys. Lett.* **2004**, *586*, 198–212.
8. G. Heusser. Low-Radioactivity Background Techniques. *Annu. Rev. Part. Nuc. Sci.* **1995**, *45*, 543.
9. Klapdor-Kleingrothaus, H.V.; Dietz, A.; Baudis, L.; Heusser, G.; Krivosheina, I.V.; Majorovits, B.; Paes, H.; Strecker, H.; Alexeev, V.; Balysh, A.; et al. Latest results from the HEIDELBERG-MOSCOW double beta decay experiment. *Eur. Phys. J.* **2001**, *A12*, 147–154.
10. Aalseth, C.E. et al. [IGEX Collaboration] IGEX  $^{76}\text{Ge}$  neutrinoless double-beta decay experiment: Prospects for next generation experiments. *Phys. Rev. D* **2002**, *65*, 092007.
11. Ackermann, K.H. et al. [GERDA Collaboration] The GERDA experiment for the search of  $0\nu\beta\beta$  decay in  $^{76}\text{Ge}$ . *Eur. J. Phys. C* **2013**, *73*, 2330.
12. Agostini, M. et al. [GERDA Collaboration] Production, characterization and operation of  $^{76}\text{Ge}$  enriched BEGe detectors in GERDA. *Eur. Phys. J. C* **2015**, *75*, 39.
13. Agostini, M.; Ur, C.A.; Budjáš, D.; Bellotti, E.; Brugnera, R.; Cattadori, C.M.; di Vacri, A.; Garfagnini, A.; Pandola, L.; Schönert, S. Signal modeling of high-purity Ge detectors with a small read-out electrode and application to neutrinoless double beta decay search in Ge-76. *J. Instrum.* **2011**, *6*, P03005.
14. Zuzel, G.; Wójcik, M.; Buck, C.; Rau, W.; Heusser, G. Ultra-traces of Ra-226 in nylon used in the BOREXINO solar neutrino experiment. *Nucl. Instr. Meth. A* **2003**, *498*, 240–255.
15. Agostini, M. et al. [GERDA collaboration] Upgrade for Phase II of the Gerda experiment. *Eur. Phys. J. C* **2018**, *78*, 388.
16. Agostini, M. et al. [GERDA collaboration] Results on neutrinoless double beta decay of  $^{76}\text{Ge}$  from GERDA Phase I. *Phys. Rev. Lett.* **2013**, *111*, 122503.
17. Agostini, M. et al. [GERDA collaboration] Improved Limit on Neutrinoless Double- $\beta$  Decay of  $^{76}\text{Ge}$  from GERDA Phase II. *Phys. Rev. Lett.* **2018**, *120*, 132503.
18. GERDA collaboration. Background-free search for neutrinoless double- $\beta$  Decay of  $^{76}\text{Ge}$  with GERDA. *Nature* **2017**, *544*, 47.
19. Agostini, M. et al. [GERDA collaboration] Improvement of the Energy Resolution via an Optimized Digital Signal Processing in GERDA Phase I. *Eur. Phys. J. C* **2015**, *75*, 255.
20. Agostini, M.; Pandola, L.; Zavarise, P. Off-line data processing and analysis for the GERDA experiment. *J. Phys. (Conf. Ser.)* **2012**, *368*, 012047.
21. Agostini, M. et al. [GERDA collaboration] Pulse shape discrimination for GERDA Phase I data. *Eur. Phys. J. C* **2013**, *73*, 2583.
22. Kotila, J.; Iachello, F. Phase space factors for double- $\beta$  decay. *Phys. Rev. C* **2012**, *85*, 034316.
23. Engel, J.; Mendez, J. Status and future of nuclear matrix elements for neutrinoless double-beta decay: A review. *Rept. Prog. Phys.* **2017**, *80*, 046301.
24. Klapdor-Kleingrothaus, H.V.; Krivosheina, I.V. The evidence for the observation of  $0\nu\beta\beta$  decay: The identification  $0\nu\beta\beta$  event form the full spectra. *Mod. Phys. Lett. A* **2006**, *21*, 1547–1566.
25. Aalseth, C.E. et al. [MAJORANA Collaboration] Search for Neutrinoless Double- $\beta$  Decay in  $^{76}\text{Ge}$  with the Majorana Demonstrator. *Phys. Rev. Lett.* **2018**, *120*, 132502.
26. Alduino, C. et al. [CUORE collaboration] First Results from CUORE: A Search for Lepton Number Violation via  $0\nu\beta\beta$  Decay of  $^{130}\text{Te}$ . *Phys. Rev. Lett.* **2018**, *120*, 132501.
27. Azzolini, O. et al. [CUPID collaboration] First Result on the Neutrinoless Double- $\beta$  Decay of  $^{82}\text{Se}$  with CUPID-0. *Phys. Rev. Lett.* **2018**, *120*, 232502.
28. Albert, J.B. et al. [EXO collaboration] Search for Neutrinoless Double-Beta Decay with the Upgraded EXO-200 Detector. *Phys. Rev. Lett.* **2018**, *120*, 072701.
29. Gando, A. et al. [KAMLAND-ZEN collaboration] Search for Majorana Neutrinos Near the Inverted Mass Hierarchy Region with KamLAND-Zen. *Phys. Rev. Lett.* **2018**, *117*, 082503.

30. Abgrall, N.; Abramov, A.; Abrosimov, N.; Abt, I.; Agostini, M.; Agartioglu, M.; Ajjaq, A.; Alvis, S.I.; Avignone, F.T., III; Bai, X.; et al. The large enriched germanium experiment for neutrinoless double beta decay (LEGEND). *AIP Conf. Proc.* **2017**, *1894*, 020027.



© 2019 by the authors. Licensee MDPI, Basel, Switzerland. This article is an open access article distributed under the terms and conditions of the Creative Commons Attribution (CC BY) license (<http://creativecommons.org/licenses/by/4.0/>).